


***P*-type ionization level lowering in ultrawide bandgap $\text{Al}_{1-x}\text{Ga}_x\text{N}$ [11 $\bar{2}$ 0] digital alloys**

Xinhao Wang¹, Jiaduo Zhu^{1,*}, Wei Shang¹, Shengrui Xu,[†] Liuying Fu, Jincheng Zhang^{1,‡} and Yue Hao
*State Key Laboratory of Wide Bandgap Semiconductor Devices and Integrated Technology, School of Microelectronics,
 Xidian University, Xi'an 710071, China*

 (Received 2 April 2024; revised 20 June 2024; accepted 26 June 2024; published 11 July 2024)

Efficient *p*-type doping is essential and challenging for applications of ultra-wide-bandgap AlGa_N with a high aluminum content. Although the band-edge-assisted ionization enabled by the superlattice of [0001] origination can reduce the ionization level due to the raised valence band maximum (VBM), the indispensable electric field induced by the spontaneous and piezoelectric polarization is in the entire range of alloy and quite negative to the photoelectric applications. In this work, we propose that band-edge-assisted ionization can be activated even without the universal electric field, which forms an ultralow ionization level of -0.1 eV for the $\text{Al}_{0.8}\text{Ga}_{0.2}\text{N}$ [11 $\bar{2}$ 0] digital alloy. The energy reduction is triggered by two factors: the intensive VBM states dominated by the coupling between GaN layers and the intriguing decrease in the unoccupied p_z level, which is induced by a symmetry reduction from C_{3v} -like to C_s at the dopant site. The transition of symmetry is triggered by a perturbation from the GaN layers, which is caused by a chainlike coupling of p_x states between nitrogen at the VBM and dopant sites and can be partially canceled depending on the dopant sites. In addition to the conventional band bending in band-edge-assisted ionization, the reduction of ionization level activated by long-ranged orbital coupling offers a new view for efficient *p*-type doping in AlGa_N systems.

DOI: [10.1103/PhysRevB.110.035202](https://doi.org/10.1103/PhysRevB.110.035202)

I. INTRODUCTION

Ultra-wide-bandgap AlGa_N with high aluminum content is greatly desired for high-power electronics and ultraviolet photonics [1–3]. Alloys of aluminum compositions above 80% enable sub-230 nm wavelength applications such as time-of-flight mass spectrometry, non-line-of-sight communication, and laser interferometer space antenna [4]. In addition, they exhibit more than 10, 700, and even 19 900 times larger Baliga figure of merit (BFOM) than GaN, GaAs, and Si, respectively [5,6]. (The BFOM is one of the benchmarks of semiconductor application in power electronics). The aluminum composition above 80% is believed to be able to effectively release the excellent performance of AlGa_N alloy [7,8].

The applications of semiconductors rely on controllable conductivity, commonly via intentional doping. By introducing *n*- and *p*-type dopants into adjacent regions of the semiconductor, a simple p-n junction can be achieved and become the cornerstone for optoelectronics devices such as light emitting diodes and photodetectors. As for the electronic devices, effective carrier extraction and injection are always required at the metal/semiconductor interfaces. Sufficient carriers should be generated by the dopants on the semiconductor side to favor the current transport. Unfortunately, the deep acceptor level above 0.4 eV in AlGa_N with an aluminum content above 80% prevents the acceptor ionization at normal temperature, which greatly impedes its applications [9]. Several methods have been adopted, including band-edge-assisted

ionization [10,11], polarization doping [12], δ doping [13], and codoping [14]. Codoping is performed by introducing the dopant couple instead of a single dopant. The coulomb attraction and the energy repulsion among individuals in the couple can lower the formation energy and the ionization level. Nevertheless, the delicate codoping configuration is usually difficult to achieve in experimental procedures. δ doping is carried out by periodically introducing a thin sheet of Mg atoms into the nitride layer to overcome the autocompensation effect and increasing the incorporation efficiency. However, the carrier transport along the vertical direction can be degraded by the dopant sheet. It also remains a challenge to achieve high hole carrier concentrations and high carrier mobilities in high Al-containing III-nitrides by this method [15]. Polarization doping is composed of an aluminum compositional grading AlGa_N and GaN layers along polar directions. The grading of the aluminum content gradually varies the polarization induced electric-field strength in the AlGa_N part; the grading heterolayers eventually induce net charges spared in the AlGa_N bulk. Band-edge-assisted ionization is performed by the transition of holes from a dopant to a raised band maximum instead of the deep valence band maximum (VBM) from the pristine bulk [16,17]. If AlGa_N alloy is made with a superlattice of ordered Al(Ga)N and GaN layers along the [0001] direction, the intrinsic polarization field can bend the band edges of Al(Ga)N and GaN in the opposite trend, so that the dopant in the wide-gap layer can be easily ionized by the raised VBM from GaN [10,18].

The polarization-dependent routes become inefficient and even negative to the photonics applications because the spontaneous and piezoelectric polarization fields along the [0001] direction can severely reduce the electron-hole recombination efficiency in photonics, usually called the quantum-confined

*Contact author: jdzhu@xidian.edu.cn

[†]Contact author: srxu@xidian.edu.cn

[‡]Contact author: jchzhang@xidian.edu.cn

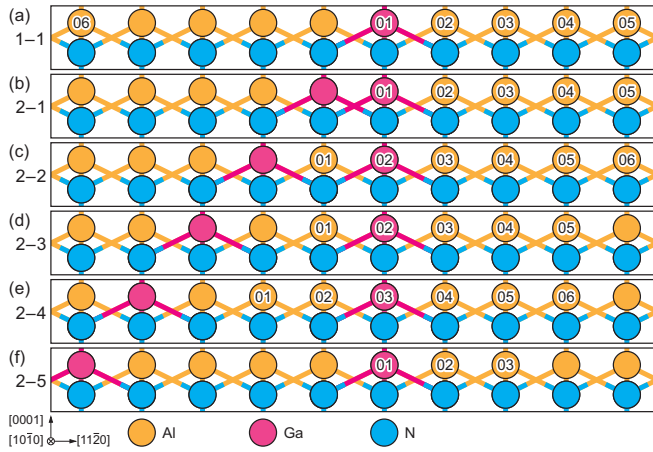


FIG. 1. Side views of the atomic arrangement of DAs with unique dopant sites.

Stark effect [19,20]. Although the nonpolar direction in the nitride can eliminate the negative effect [21], the activation of p type in nonpolar AlGa \bar{N} is still a challenge. In particular, without help from intrinsic electric field-induced band bending, whether the band-edge-assisted ionization can be activated is completely unknown.

In this work, we propose that band-edge-assisted ionization can be activated in $[11\bar{2}0]$ Al $_{0.9}$ Ga $_{0.1}$ N and Al $_{0.8}$ Ga $_{0.2}$ N short-period superlattice by reducing the unoccupied acceptor level in addition to the natural valence band offsets (VBO) between AlN and GaN. This approach leads to an ultralow activation energy level of -0.1 eV in Al $_{0.8}$ Ga $_{0.2}$ N, which is even lower than the best result of digital alloy (DA) along the $[0001]$ direction. By eliminating the electric field induced band bending, an unusual symmetry lowering induced by the coupling between VBM and dopant sites is responsible for the acceptor level reduction.

II. COMPUTATIONAL METHOD

The short-period superlattice of AlGa \bar{N} $[11\bar{2}0]$ DA was built by enumerating the dopant sites and alloy structures at the 0.9 and 0.8 aluminum compositions. As shown in Fig. 1, $6 \times 5 \times 3$ wurtzite supercells containing 360 atoms with 10 GaN monolayers (MLs) were adopted. There are 1 (6) and 5 (25) alloy structures (dopant sites) for Al $_{0.9}$ Ga $_{0.1}$ N and Al $_{0.8}$ Ga $_{0.2}$ N DA, respectively. Here, we ordinarily use Mg as the p -type dopant. All calculations were performed using density functional theory (DFT) with the PWmat package [22,23]. The exchange-correlation potential was described by the Perdew-Burke-Ernzerhof (PBE) functional with the generalized gradient approximation (GGA) [24]. The HSE06 hybrid functional correction with an alpha value of 0.38 was considered for the correct bandgap [25,26]. The PD04 optimized norm-conserving Vanderbilt (ONCV) pseudopotential was adopted with an energy cutoff of 60 Ry [27]. For the relaxation of unicells, the density of the sampling mesh for the integration in the Brillouin zone was 0.25 \AA^{-1} . The relaxation criterion for the atomic displacement was 0.02 eV/\AA .

The formation energy of a defect/impurity α in charge state q is [28]

$$\Delta H(\alpha, q) = E(\alpha, q) - E(\text{host}) - \sum_i n_i (E_i + \mu_i) + q[E_{\text{VBM}}(\text{host}) + E_F + \Delta V], \quad (1)$$

where $\Delta H(\alpha, q)$ and $E(\alpha, q)$, which are functions of defect/impurity type α and charge q , are the formation and total energy of the system, respectively. $E(\text{host})$ is the energy of the corresponding host (or bulk) system. n_i , E_i , and μ_i are the number, energy, and chemical potential of atom i . Referring to the host system, $n_i > 0$ if one adds an atom to the system; $n_i < 0$ if one removes an atom from the system. $E_{\text{VBM}}(\text{host})$ and E_F are VBM energy and the Fermi energy level of the host system and new system, respectively. ΔV is the potential correction. Due to thermodynamical constraints, the chemical potentials are confined by Eqs. (2)–(4):

$$\mu_X + \mu_N = \Delta H(\text{XN}), \quad X = \text{Al, Ga}, \quad (2)$$

$$2\mu_{\text{Mg}} + 3\mu_N \leq \Delta H(\text{Mg}_2\text{N}_3), \quad (3)$$

$$\mu_i \leq 0, \quad i = \text{Al, Ga, Mg, N}. \quad (4)$$

Equation (2) is an equation instead of the usual inequality because we assume that such alloy structures are grown layer by layer toward the $[11\bar{2}0]$ direction. The activation energy level is defined as the Fermi energy at which charge states $q = 0$ and $q = -1$ have equal formation energy, and it is calculated as follows:

$$E_a = E(\alpha, -1) - E(\alpha, 0) - [E_{\text{VBM}}(\text{host}) + \Delta V]. \quad (5)$$

Only low-charge states of -1 were considered, and the nonhomogeneous dielectric constant in the DAs was contributed by various combinations of GaN and AlN layers. Thus, alignment for the electrostatic interactions among finite-sized charged supercells was not adopted.

III. RESULTS AND DISCUSSION

Figures 2(a) and 2(b) show the bandgap and mixing enthalpy values, respectively. The bandgap of Al $_{0.9}$ Ga $_{0.1}$ N is 5.74 eV, which is consistent with the conventional AlGa \bar{N} alloy [29]. For Al $_{0.8}$ Ga $_{0.2}$ N, the coupling between GaN layers reduces the bandgap values from 5.49 eV in 2–5 to 5.23 eV in 2–1. The calculated value range is also consistent with the experimental report of 5.3 eV [30]. At the compositional level, the evolution of the mixing enthalpy follows the experimental trend, since Al $_{0.8}$ Ga $_{0.2}$ N DAs generally have higher values than Al $_{0.9}$ Ga $_{0.1}$ N DA. Furthermore, the coupling between GaN layers slightly favors the stability, so 2–1 is the best candidate for growth among Al $_{0.8}$ Ga $_{0.2}$ N DAs.

The formation energy of dopants is first evaluated at the nonionized level under the nitrogen-rich condition. As illustrated in Fig. 3(a), substitution at the gallium sites is always the most preferred option and the aluminum sites at the first neighbor of the GaN layers are the second preference. When the dopant moves to further neighbor sites, the formation energy first increases and subsequently quickly converges, which suggests a weakening of the influence from the GaN

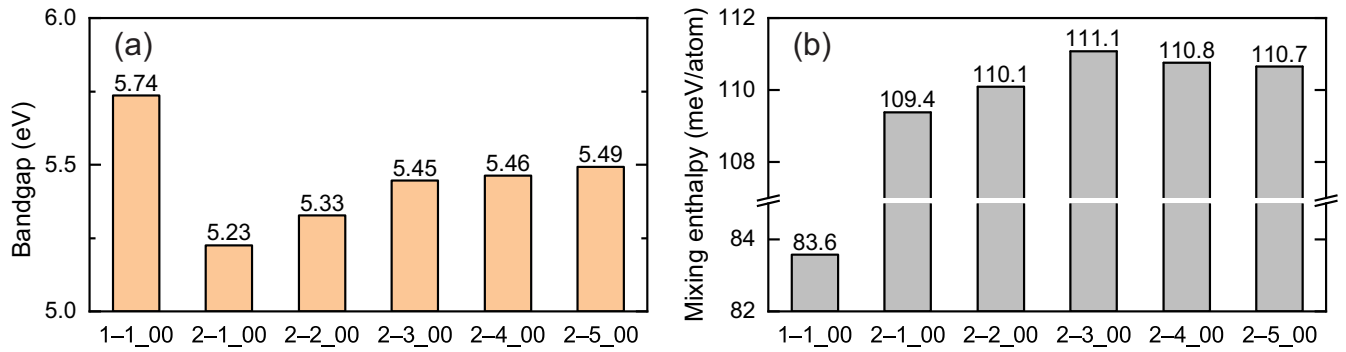


FIG. 2. (a) Bandgap and (b) mixing enthalpy of DAs.

layers. The influence also evolves at the aluminum sites at the inner side between two GaN layers. When the GaN layers are separated by fewer than four layers, the sites on the inner side generally do not have higher formation energy than the mirror sites on the outer side. The energy difference between mirror sites tends to vanish when the two GaN layers gradually separate. Since the radii of Mg, Ga, and Al are 145 pm, 136 pm, and 118 pm, respectively, the trends of the formation energy as a function of the dopant site can be attributed to the balance between expansion and shrinkage of nitrogen around the GaN and AlN layers, respectively.

Then, the activation energy level can be calculated by considering the transition between charge states from $q = 0$ to $q = -1$, which leads to a hole ionization in the latter case. As shown in Fig. 3(b), substitution at the gallium sites always yields quite difficult p -type ionization. The energy level approaches 0.6 eV, since the GaN layers are separated by more than 1 layer (including 1-1). The values reduce to 0.46 and 0.38 eV for the 2-1 and 2-2 configurations, respectively, which remain higher than those in the pristine GaN bulk. The increase in energy level at the GaN parts can be attributed to the strong perturbation from the AlN layers, which can be weakened by enhancing the coupling

between GaN layers. For substitution at aluminum sites, the dopant at the first neighbor site can never lead to a low energy level, although the VBM is spatially closest to the dopant. Interestingly, evident energy reduction always occurs with the motion from the second neighbor to further aluminum sites. The best result is 0.4 eV for $\text{Al}_{0.9}\text{Ga}_{0.1}\text{N}$, which is slightly lower than 0.47 eV in the conventional alloy of the same composition [31]. For $\text{Al}_{0.8}\text{Ga}_{0.2}\text{N}$, the energy reduction can be enhanced by the coupling between GaN layers, which causes fascinating results of -0.1 eV and 0.03 eV in the 2-1 and 2-2 configurations, respectively. The former is even much lower than the empirical record of 17 meV in the [0001] oriented $\text{Al}_{0.63}\text{Ga}_{0.37}\text{N}$ short period superlattice [32]. When the GaN layers are gradually separated, the averaged energy levels increase and converge to the values of $\text{Al}_{0.9}\text{Ga}_{0.1}\text{N}$.

To understand the activation energy level trend, the energy difference between the unoccupied p_z states of nitrogen at the dopant and the VBM was extracted from eigenvalues and denoted as the activation energy E_a in the single-particle picture. All values in each DA were shifted with the same offset to make E_a at the gallium sites a reference. Moreover, we divided the band edge-assisted ionization into two levels: site level and atomic relaxation level, which correspond to the position of the dopant relative to the GaN layer (i.e., VBM) and the relaxation of atomic bonds, respectively. First, the site-level effect was evaluated by only taking the substitution without relaxation.

As shown in Fig. 4(a), the first neighbor aluminum site of the GaN layer can hardly induce a decrease in energy level. The effect can be enhanced at the aluminum sites deep in the AlN layers due to the VBO between GaN and AlN. In addition to the dopant sites, the arrangement of the GaN layer exhibits a more severe effect. In the DA with separated GaN layers, the congregation of GaN layers can induce more energy decrease. Since the interfacial coupling between adjacent AlN layers can fuzz the VBM state contribution from the GaN single layer (see Fig. S1 in the Supplemental Material [33]), the energy decrease is derived from the enhanced VBM from a coupling between GaN layers. However, band edge-assisted ionization cannot be sufficiently triggered at the site-level effect, even with an evident VBO between GaN and AlN layers in the 2-1 configuration.

As shown in Fig. 4(b), with additional atomic bond relaxation, the first neighbor aluminum sites remain insufficient to

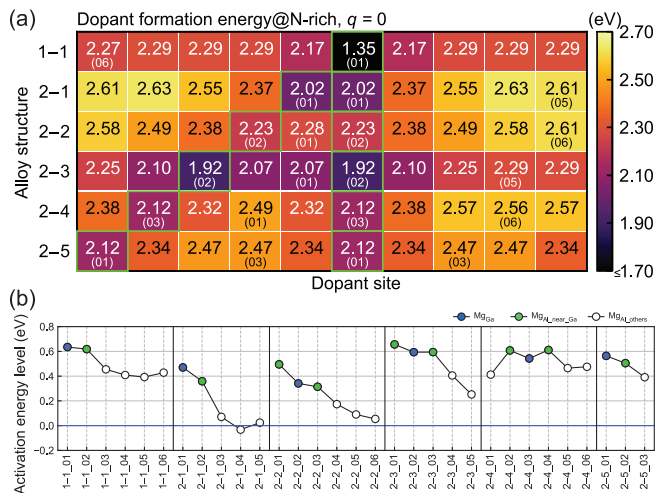


FIG. 3. (a) Formation energy at the nonionized state and (b) the activation energy level of Mg dopants in AlGaIn DAs.

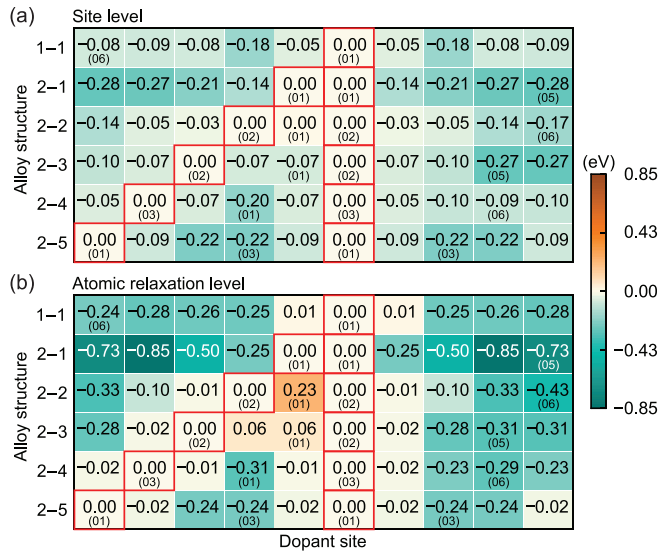


FIG. 4. Relative reduction of E_a at the (a) site and (b) atomic relaxation levels, respectively. E_a at the gallium sites is shifted to 0 eV as a reference in the same DA.

trigger an efficient energy reduction and can even negatively impact the ionization. The relaxation effect from two adjacent GaN layers increases the energy levels by 0.23 and 0.06 eV for the inside aluminum sites of 2-2 and 2-3 configurations, respectively. Moving from the first to further aluminum sites, we can observe a noticeable reduction in energy levels in the outside regions (see Figs. S2–S7 in the Supplemental Material [33]). Moreover, decreasing the space between GaN layers reduces the energy more than other separated cases because intensive VBM states arise from the interfacial coupling. A robust band edge intensity is accordingly essential for the band edge-assisted ionization at both site and atomic relaxation levels. Consequently, evident E_a reduction of 0.7 eV is achieved at the 2-1_04 and 2-1_05 configurations, and the acceptor level in these sites resonates with the VBM states at GaN layers, which indicates the activation of band edge-assisted ionization. The band edge-assisted energy level reduction can be effectively activated by atomic relaxation at the appropriate dopant sites.

The N-Mg bond length around the dopant was extracted to understand the atomic relaxation effect. As shown in Fig. 5, due to the C_{3v} symmetry in wurtzite nitride, the four N-Mg bonds can be separated into two groups: the c_{\parallel}^0 bond along

the [0001] direction and three short c_{\perp}^1 , c_{\perp}^2 , and c_{\perp}^3 bonds. The c_{\parallel}^0 (c_{\perp}^1 , c_{\perp}^2 , and c_{\perp}^3) bonds in $\text{Al}_{0.9}\text{Ga}_{0.1}\text{N}$ is averaged longer (shorter) than $\text{Al}_{0.8}\text{Ga}_{0.2}\text{N}$. The stronger hybridization in the three N-Mg bonds leads to a more localized p_z orbital derived from the c_{\parallel}^0 bond [34]. Therefore, E_a in $\text{Al}_{0.9}\text{Ga}_{0.1}\text{N}$ is generally higher than $\text{Al}_{0.8}\text{Ga}_{0.2}\text{N}$. Similarly, the c_{\perp}^1 , c_{\perp}^2 , and c_{\perp}^3 bonds at the first neighbor aluminum sites are generally shorter than other dopant sites in the same DA, which indicates that the strain from the neighbor GaN layer can enhance the p_x and p_y coupling in the N-Mg bonding. The more covalent bond pushes the Mg_{Al} level upward [35], which cancels the site effect and even leads to a higher energy than the neighbor Mg_{Ga} at the first neighbor aluminum sites inside. The strain between AlN and GaN layers weakens when the dopant site moves further, which eventually reduces the symmetry from quasi- C_{3v} at the first neighbor Al sites to C_s at the farthest site. During the transformation from quasi- C_{3v} to C_s , the bond length of c_{\perp}^1 and c_{\perp}^2 asymmetrically evolves. The c_{\perp}^1 bonds toward the GaN layers are stretched slower than c_{\perp}^2 bonds. Because Mg_{Al} in the AlN bulk remains C_{3v} symmetric, the symmetry reduction and asymmetric stretch between c_{\perp}^2 and c_{\perp}^1 bonds suggest that there is an additional perturbation against strain from GaN among all dopant sites. The c_{\perp}^1 and c_{\perp}^2 bonds have equal lengths at the 2-2_01 site, which suggests that the strain and perturbation reach a balance at the middle dopant sites between GaN layers. Moreover, the symmetry of the farthest site 1-1_06 is closer to C_{3v} than the corresponding sites in the 2-X systems, which indicates that the perturbation favored by E_a reduction should derive from the GaN layer.

To understand the perturbation effects, energy-level decomposed wave function around the Fermi level were extracted from the 2-1_05 configuration due to their strongest VBM states with the furthest dopant site. As shown in Fig. 6, the VBM was derived from p_z orbitals of nitrogen atoms at the GaN layers. Due to the slight strain, the sub-VBM states of the degenerate p_x and p_y orbitals split with 0.2 eV. Without perturbation from VBM, a large energy gap exists between occupied p_x and unoccupied p_z of nitrogen around the dopant. The perturbation is caused by a chainlike p_x coupling between dopant and VBM sites along the [1120] direction. At the dopant site, the coupling is responded by a stretch of two N-Mg bonds c_{\perp}^1 and c_{\perp}^2 . The coupling also leads to an energy raise of the p_x orbitals (see Fig. S8 in the Supplemental Material [33]). This variation in the sp^3 configuration weakens the repulsion at the p_z orbital and eventually reduces the activation energy level.

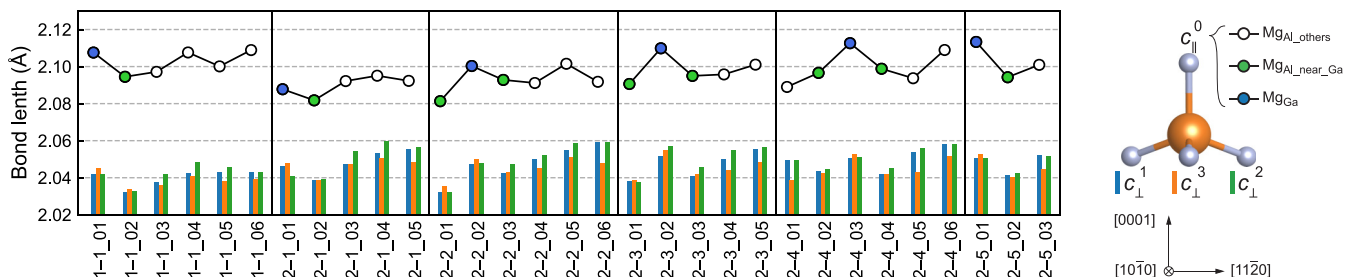


FIG. 5. N-Mg bond length at dopant sites in each DA.

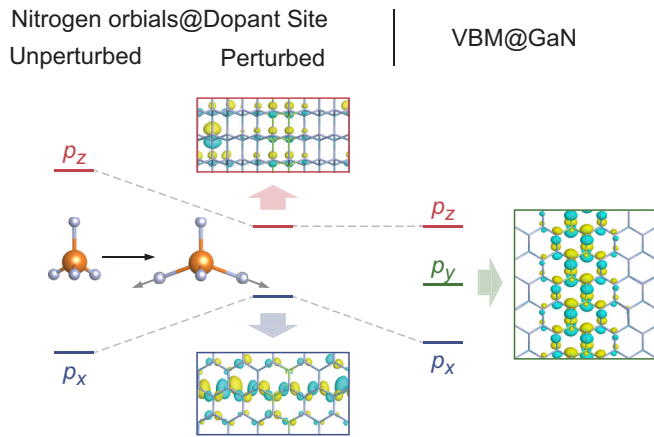


FIG. 6. Energy level diagram and the corresponding wave function of 2-1_05.

Although the best dopant configuration presents a high formation energy, the doping process is practical for growth. The 2-1 configuration presents the lowest mixing enthalpy for $\text{Al}_{0.8}\text{Ga}_{0.2}\text{N}$, which is favored for growth. The dopant site can be controlled by adjusting the Mg flux during the growth. The formation energy also suggests that the incorporation can be more active than other configurations in most chemical windows (see Fig. S9 in the Supplemental Material [33]). Recently, from the fabrication aspect, Lucie Valera *et al.* [36] inspiringly achieved AlGaN digital alloy toward nonpolar direction by MOCVD; the favorable MBE based metal modulated epitaxy (MME) method is also expect to conjointly grow the presented DAs in high quality with proper control of the Mg distribution [32,37-39]. Therefore, we proposed a possible route to grow the proposed configurations. As shown in Fig. 7, the desired DA with the appropriate dopant site can be possibly achieved by periodical switching of the metal source shutters. With pressure and substrate temperature control, interfacially sharp atomic layers could be deposited. The main challenge could still be the AlN [11 $\bar{2}$ 0] buffer layer, which is usually grown on the *r*-plane sapphire. Thanks to the repaid progress of AlN bulk growth technology, the possible adoption of AlN [11 $\bar{2}$ 0] substrate can be much favored for the DA growth in the future.

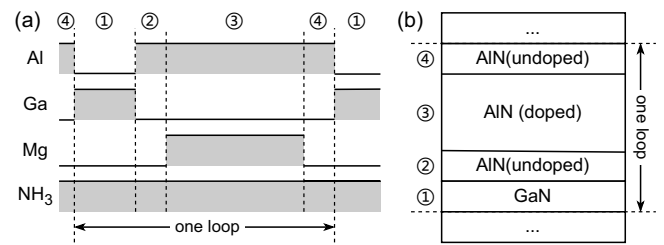


FIG. 7. Schematic of growing [11 $\bar{2}$ 0] *p*-type AlGaN DAs. (a) Schematic process; (b) Schematic illustration of the DA structure for one loop.

IV. CONCLUSIONS

In conclusion, band edge-assisted *p*-type ionization in $\text{Al}_{0.9}\text{Ga}_{0.1}\text{N}$ and $\text{Al}_{0.8}\text{Ga}_{0.2}\text{N}$ DAs along the nonpolar [11 $\bar{2}$ 0] direction was systematically investigated by enumerating the magnesium dopant sites and alloy structures. The best activation energy levels are 0.4 and -0.1 eV for $\text{Al}_{0.9}\text{Ga}_{0.1}\text{N}$ and $\text{Al}_{0.8}\text{Ga}_{0.2}\text{N}$, respectively. The effective band edge-assisted ionization can be activated by two factors: the intensive VBM states contributed by the coupling between GaN layers; the symmetry decrease at the dopant sites induced by the coupling of nitrogen p_x orbitals between VBM and dopant sites. Compared to symmetry preserving in the conventional views [34,40], it is interesting that the acceptor level can be reduced by symmetry lowering which is carried out by coupling of $2p$ orbitals between anions at the dopant and the VBM sites. Since anions' p orbitals contribute to the VBM of most semiconductors, we suggest the route is promising to overcome *p*-type doping bottleneck in other ternary semiconductors of ultrawide bandgaps. For example, *p*-type doping is extremely difficult in $(\text{Al}_x\text{Ga}_{1-x})_2\text{O}_3$ alloys [41]. If the alloy can be grown as a digital alloy, carefully designing the order of the binary oxide and the dopant sites under a specific crystal direction, the coupling between the dopant and VBM sites can be varied and defect level energy reduction may be activated.

ACKNOWLEDGMENTS

Authors are grateful for the support by the National Key R&D Program of China Grant No. (2022YFB3605401), the National Natural Science Foundation of China Grants No. (No. 62127812 and No. 61925404), and the Natural Science Basic Research Program of Shaanxi (No. 2023-JC-JQ-56).

- [1] Y. Zhang, J. Zhang, Z. Liu, S. Xu, K. Cheng, J. Ning, C. Zhang, L. Zhang, P. Ma, H. Zhou, and Y. Hao, Demonstration of a 2 kV $\text{Al}_{0.85}\text{Ga}_{0.15}\text{N}$ Schottky barrier diode with improved on-current and ideality factor, *IEEE Electron Device Lett.* **41**, 457 (2020).
- [2] Q. Cai, H. You, H. Guo, J. Wang, B. Liu, Z. Xie, D. Chen, H. Lu, Y. Zheng, and R. Zhang, Progress on AlGaN-based solar-blind ultraviolet photodetectors and focal plane arrays, *Light Sci. Appl.* **10**, 94 (2021).
- [3] C. Reich, M. Guttmann, M. Feneberg, T. Wernicke, F. Mehnke, C. Kuhn, J. Rass, M. Lapeyrade, S. Einfeldt, A. Knauer, V. Kueller, M. Weyers, R. Goldhahn, and M. Kneissl, Strongly

transverse-electric-polarized emission from deep ultraviolet AlGaN quantum well light emitting diodes, *Appl. Phys. Lett.* **107**, 142101 (2015).

- [4] M. Kneissl, T.-Y. Seong, J. Han, and H. Amano, The emergence and prospects of deep-ultraviolet light-emitting diode technologies, *Nat. Photonics* **13**, 233 (2019).
- [5] J. Y. Tsao, S. Chowdhury, M. A. Hollis, D. Jena, N. M. Johnson, K. A. Jones, R. J. Kaplar, S. Rajan, C. G. Van De Walle, E. Bellotti, C. L. Chua, R. Collazo, M. E. Coltrin, J. A. Cooper, K. R. Evans, S. Graham, T. A. Grotjohn, E. R. Heller, M. Higashiwaki, M. S. Islam, P. W. Juodawlkis, M. A. Khan, A. D.

- Koehler, J. H. Leach, U. K. Mishra, R. J. Nemanich, R. C. N. Pilawa-Podgurski, J. B. Shealy, Z. Sitar, M. J. Tadjer, A. F. Witulski, M. Wraback, and J. A. Simmons, Ultrawide-bandgap semiconductors: Research opportunities and challenges, *Adv. Electron. Mater.* **4**, 1600501 (2018).
- [6] K. A. Jones, T. P. Chow, M. Wraback, M. Shatalov, Z. Sitar, F. Shahedipour, K. Udary, and G. S. Tompa, AlGaIn devices and growth of device structures, *J. Mater. Sci.* **50**, 3267 (2015).
- [7] S. Bajaj, T.-H. Hung, F. Akyol, D. Nath, and S. Rajan, Modeling of high composition AlGaIn channel high electron mobility transistors with large threshold voltage, *Appl. Phys. Lett.* **105**, 263503 (2014).
- [8] A. M. Armstrong and A. A. Allerman, Polarization-induced electrical conductivity in ultra-wide band gap AlGaIn alloys, *Appl. Phys. Lett.* **109**, 222101 (2016).
- [9] M. S. Hasan, I. M. Mehedi, S. M. F. Reza, M. R. Kaysir, and M. R. Islam, Analytical investigation of activation energy for Mg-doped p-AlGaIn, *Opt. Quantum Electron.* **52**, 348 (2020).
- [10] E. F. Schubert, W. Grieshaber, and I. D. Goepfert, Enhancement of deep acceptor activation in semiconductors by superlattice doping, *Appl. Phys. Lett.* **69**, 3737 (1996).
- [11] P. Bogusławski, N. G. Szwacki, and J. Bernholc, Interfacial segregation and electrodiffusion of dopants in AlN / GaN superlattices, *Phys. Rev. Lett.* **96**, 185501 (2006).
- [12] J. Simon, V. Protasenko, C. Lian, H. Xing, and D. Jena, Polarization-induced hole doping in wide-band-gap uniaxial semiconductor heterostructures, *Science* **327**, 60 (2010).
- [13] C. Bayram, J. L. Pau, R. McClintock, and M. Razeghi, Delta-doping optimization for high quality p-type GaN, *J. Appl. Phys.* **104**, 083512 (2008).
- [14] R. Q. Wu, L. Shen, M. Yang, Z. D. Sha, Y. Q. Cai, Y. P. Feng, Z. G. Huang, and Q. Y. Wu, Enhancing hole concentration in AlN by Mg:O codoping: *Ab Initio* study, *Phys. Rev. B* **77**, 073203 (2008).
- [15] Y.-H. Liang and E. Towe, Progress in efficient doping of high aluminum-containing group III-nitrides, *Appl. Phys. Rev.* **5**, 011107 (2018).
- [16] Y. Yan, J. Li, S.-H. Wei, and M. M. Al-Jassim, Possible approach to overcome the doping asymmetry in wideband gap semiconductors, *Phys. Rev. Lett.* **98**, 135506 (2007).
- [17] K. Jiang, X. Sun, Z. Shi, H. Zang, J. Ben, H.-X. Deng, and D. Li, Quantum engineering of non-equilibrium efficient p-doping in ultra-wide band-gap nitrides, *Light Sci. Appl.* **10**, 69 (2021).
- [18] K. Ebata, J. Nishinaka, Y. Taniyasu, and K. Kumakura, High hole concentration in Mg-doped AlN/AlGaIn superlattices with high Al content, *Jpn. J. Appl. Phys.* **57**, 04FH09 (2018).
- [19] D. A. B. Miller, D. S. Chemla, T. C. Damen, A. C. Gossard, W. Wiegmann, T. H. Wood, and C. A. Burrus, Band-edge electroabsorption in quantum well structures: The quantum-confined stark effect, *Phys. Rev. Lett.* **53**, 2173 (1984).
- [20] T. Takeuchi, S. Sota, M. Katsuragawa, M. Komori, H. Takeuchi, H. A. Hiroshi Amano, and I. A. Isamu Akasaki, Quantum-confined stark effect due to piezoelectric fields in GaInN strained quantum wells, *Jpn. J. Appl. Phys.* **36**, L382 (1997).
- [21] P. Waltereit, O. Brandt, A. Trampert, H. T. Grahn, J. Menniger, M. Ramsteiner, M. Reiche, and K. H. Ploog, Nitride semiconductors free of electrostatic fields for efficient white light-emitting diodes, *Nature (London)* **406**, 865 (2000).
- [22] W. Jia, Z. Cao, L. Wang, J. Fu, X. Chi, W. Gao, and L.-W. Wang, The analysis of a plane wave pseudopotential density functional theory code on a GPU machine, *Comput. Phys. Commun.* **184**, 9 (2013).
- [23] W. Jia, J. Fu, Z. Cao, L. Wang, X. Chi, W. Gao, and L.-W. Wang, Fast plane wave density functional theory molecular dynamics calculations on multi-GPU machines, *J. Comput. Phys.* **251**, 102 (2013).
- [24] J. P. Perdew, K. Burke, and M. Ernzerhof, Generalized gradient approximation made simple, *Phys. Rev. Lett.* **77**, 3865 (1996).
- [25] J. Heyd, G. E. Scuseria, and M. Ernzerhof, Hybrid functionals based on a screened coulomb potential, *J. Chem. Phys.* **118**, 8207 (2003).
- [26] A. V. Krukau, O. A. Vydrov, A. F. Izmaylov, and G. E. Scuseria, Influence of the exchange screening parameter on the performance of screened hybrid functionals, *J. Chem. Phys.* **125**, 224106 (2006).
- [27] D. R. Hamann, Optimized norm-conserving Vanderbilt pseudopotentials, *Phys. Rev. B* **88**, 085117 (2013).
- [28] S.-H. Wei, Overcoming the doping bottleneck in semiconductors, *Comput. Mater. Sci.* **30**, 337 (2004).
- [29] N. Nepal, J. Li, M. L. Nakarmi, J. Y. Lin, and H. X. Jiang, Temperature and compositional dependence of the energy band gap of AlGaIn alloys, *Appl. Phys. Lett.* **87**, 242104 (2005).
- [30] D. Brunner, H. Angerer, E. Bustarret, F. Freudenberger, R. Höppler, R. Dimitrov, O. Ambacher, and M. Stutzmann, Optical constants of epitaxial AlGaIn films and their temperature dependence, *J. Appl. Phys.* **82**, 5090 (1997).
- [31] M. L. Nakarmi, N. Nepal, J. Y. Lin, and H. X. Jiang, Photoluminescence studies of impurity transitions in Mg-doped AlGaIn alloys, *Appl. Phys. Lett.* **94**, 091903 (2009).
- [32] J. Wang, M. Wang, F. Xu, B. Liu, J. Lang, N. Zhang, X. Kang, Z. Qin, X. Yang, X. Wang, W. Ge, and B. Shen, Sub-nanometer ultrathin epitaxy of AlGaIn and its application in efficient doping, *Light Sci. Appl.* **11**, 71 (2022).
- [33] See the Supplemental Material at <http://link.aps.org/supplemental/10.1103/PhysRevB.110.035202> for (i) Fig. S1. Projected local density of states (PLDOS) of Bulk AlGaIn DAs; (ii) Figures S2–S7. PLDOS of doped AlGaIn DAs; (iii) Figure S8. PDOS of low activation energy dopant sites. (iv) Figure S9. Formation energy of doped AlGaIn DAs.
- [34] J. L. Lyons, A. Janotti, and C. G. Van De Walle, Impact of group-II acceptors on the electrical and optical properties of GaN, *Jpn. J. Appl. Phys.* **52**, 08JJ04 (2013).
- [35] X. Cai, J. Yang, P. Zhang, and S.-H. Wei, Origin of deep acceptor levels in nitride semiconductors: The roles of chemical and strain effects, *Phys. Rev. Appl.* **11**, 034019 (2019).
- [36] L. Valera, V. Grenier, S. Finot, C. Bougerol, J. Eymery, G. Jacopin, and C. Durand, M-plane AlGaIn digital alloy for microwire UV-B LEDs, *Appl. Phys. Lett.* **122**, 141101 (2023).
- [37] H. Ahmad, J. Lindemuth, Z. Engel, C. M. Matthews, T. M. McCrone, and W. A. Doolittle, Substantial p-type conductivity of AlN achieved via beryllium doping, *Adv. Mater.* **33**, 2104497 (2021).
- [38] H. Ahmad, T. J. Anderson, J. C. Gallagher, E. A. Clinton, Z. Engel, C. M. Matthews, and W. Alan Doolittle, Beryllium doped semi-insulating GaN without surface accumulation for homoepitaxial high power devices, *J. Appl. Phys.* **127**, 215703 (2020).

- [39] H. Ahmad, T. J. Anderson, J. C. Gallagher, E. A. Clinton, Z. Engel, C. M. Matthews, and W. Alan Doolittle, Publisher's Note: "Beryllium doped semi-insulating GaN without surface accumulation for homoepitaxial high power devices" [J. Appl. Phys. **127**, 215703 (2020)], [J. Appl. Phys. **128**, 079902 \(2020\)](#).
- [40] D. Segev and S.-H. Wei, Design of shallow donor levels in diamond by isovalent-donor coupling, [Phys. Rev. Lett. **91**, 126406 \(2003\)](#).
- [41] H. Peelaers, J. B. Varley, J. S. Speck, and C. G. Van de Walle, Structural and electronic properties of $\text{Ga}_2\text{O}_3\text{-Al}_2\text{O}_3$ alloys, [Appl. Phys. Lett. **112**, 242101 \(2018\)](#).